The development of a computational platform to design and simulate on-board hydrogen storage systems

Mazzucco, Andrea; Rokni, Masoud

Published in:
International Journal of Hydrogen Energy

Link to article, DOI:
10.1016/j.ijhydene.2016.10.051

Publication date:
2017

Document Version
Peer reviewed version

A Mazzucco, M Rokni. The Development of a Computational Platform to Design and Simulate On-Board Hydrogen Storage Systems. Hydrogen Energy 2017;42:2187 - 2200.

The development of a computational platform to design and simulate on-board hydrogen storage systems

Andrea Mazzucco, Masoud Rokni*

Department of Mechanical Engineering
Technical University of Denmark, Nils Koppels Allé 403, DK-2800 Kongens-Lyngby, Denmark
andmaz@mek.dtu.dk; mr@mek.dtu.dk

Abstract
A computational platform is developed in the Modelica® language within the Dymola™ environment to provide a tool for the design and performance comparison of on-board hydrogen storage systems. The platform has been coupled with an open source library for hydrogen fueling stations to investigate the vehicular tank within the frame of a complete refueling system. The two technologies that are integrated in the platform are solid-state hydrogen storage in the form of metal hydrides and compressed gas systems. In this work the computational platform is used to compare the storage performance of two tank designs based on the tubular tank configuration with $Ti_{1.1}CrMn$ as the absorbing alloy. Results show that a shell and tube layout with metal hydride tubes of 2 mm inner diameter achieves the desired refueling time of 3 min and store a maximum of 3.1 kg of hydrogen in a 126 L tank, corresponding to a storage capacity four times larger than a tube-in-tube solution of the same size. The volumetric and gravimetric densities of the shell and tube are 2.46% and 1.25% respectively. The dehydriding ability of this solution is proven to withstand intense discharging conditions.

Keywords: Modelica; hydrogen storage; computational platform; dynamic model; heat transfer; metal hydride.

1. Introduction

The transportation sector accounts for approximately 14% of the global emissions of greenhouse gases (GHGs), two thirds of which come from road transportation, which is entirely dependent upon fossil fuels and was responsible for 112 million metric tons of equivalent CO_2 in 2014 [1]. Therefore, a clean alternative to current gasoline cars can provide a substantial benefit in terms of GHG reduction and global warming mitigation. One of these clean technologies is the fuel cell electric vehicle (FCEV). Despite the recent commercialization of FCEVs [2], [3], many challenges have yet to be overcome in order to establish a solid ground for a significant market penetration of such a technology. The development of an effective solution for on-board hydrogen storage is one of the main technical tasks that need to be tackled [4], [5].

This study presents the Hydrogen Storage and Design Platform (HySDeP), which is intended to serve as a simulation tool to design and compare different vehicular storage options with respect to targets based upon storage and fueling efficiencies, providing a starting point for a comprehensive model library that includes the main on-board storage solutions.

*Corresponding author

Attention is given to solutions that involve hydrogen storage in metal hydride tanks and compressed hydrogen gas (CHG) vessel with an integrated phase change material (PCM) as the passive cooling system. A set of libraries is implemented in the modeling platform to select among different material compositions, kinetic equations, heat exchanger configurations and to enable the tailoring of the analysis according to the user needs. An ongoing effort is focusing on expanding such libraries and also including other types of tank configurations. The next step in this direction is to use the developed models to design MH tanks based on the chamber layout and different heat exchanger configurations that can be selected from a wide library. In addition, the effect of performance degradation over charging/discharging cycles is planned to be included in the next platform version.

Reliable computational models are developed to describe hydriding and dehydriding reactions as well as melting and solidification processes that occur in the metal hydride tank and novel compressed-hydrogen vessel respectively [6], [7]. For the former, these models are used to quantify the main design parameter, being the critical metal hydride thickness, for the tank/heat-exchanger system as described in the *Heat exchanger designs* Section and in more detail in Ref. [6], wherein a verification of the model is also provided. Only the main results that refer to the MHSS are here presented, as the analysis of the CHG system was discussed in Ref. [7].

This work focuses on the charging and discharging processes of MHSSs to investigate the storage performance of two tank/heat-exchanger systems implemented in HySDeP. The gravimetric and volumetric densities, storage capacity as well as time of refueling/discharging are evaluated to select the most promising layout. Finally, a sensitivity analysis on the main geometrical parameters is carried out to address the advantages and limitations of each configuration and identify strategies for further improvement.

2. Methods

In this section we describe the methodology used to design the computational platform and set up the charging and discharging analyses presented in this work. In addition, it is made possible to couple the platform with the hydrogen refueling station library presented in Ref. [8] to investigate the different storage options within the frame of a complete refueling system. The platform can be freely downloaded from the github repository of the *DTU-TES* group [9].

2.1 Design of the simulation platform

The design approach of the platform is based on three criteria, such as:

- flexibility;
- user friendliness;
- ease of third party development.

These concepts are chosen to make the platform work as both a design/simulation tool for users and a well-structured environment for model developers. This means that the platform should be designed to adapt the needs of different users and should be based on an efficient and clear architecture in order to ease the code modification. In order to make the use of the platform as straightforward as possible for both types of end-users, its design is based on a multi-level architecture.

The first level corresponds to the *macro*-models representing the main physical components. Such components correspond to containers within which multiple nested sub-models are defined to perform intermediate calculation tasks. These sub-models represent the second level of hierarchy. The user

should have direct access only to the *macro*-components. This occurs via the graphical interface, through which the domain of investigation and the values for the input parameters can be defined. To simplify the user interaction with the platform, the number of macro-models is limited to three, namely *Ambient*, *Refueling station* and the tank system. The developer should have access to both levels in order to modify the structure and operation of the platform. Different *if* -scenarios guide the user through the model set up, enabling the selection of various options and thus, the tailoring of the analysis based on specific needs. The first choice the user is asked to take, refers to which storage system should be investigated: MHSS or CHG-tank with or without PCM.

The component hierarchy should be implemented with preference for constructs that keep the modeling approach as simple and intuitive as possible. In Modelica® the above preference translates in the use of *inner*/*outer* and port/connector elements rather than nested *extends* constructs to exchange constant and variables between models. In addition, the code should be well commented to ease the understanding of all the implemented features. A reference list is included at the end of each component code to make transparent the source of equations, thermo-physical properties, thermal models and assumptions. These aspects are of fundamental importance as the platform should in principle allow for its use and modification by different users, including both company employees and researchers. In Fig. 1 the platform structure is shown in view of its *macro*-components and main implemented features.

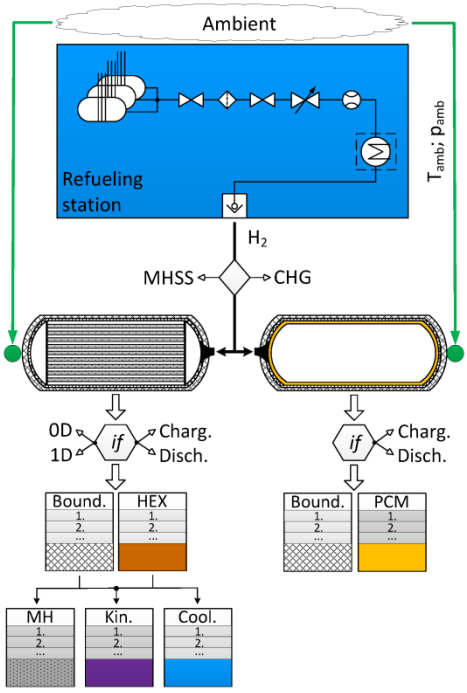

Figure 1: Modeling platform. Architecture concept.

Fig. 1 should be read as a black box scheme where the main components and information flows are presented. A more detailed description of the sub-models contained inside each *macro*-component can be found in Ref. [10], whereas the entries of the libraries presented in such a figure are reported in Appendix A. The ambient model serves as the environment where the user defines the ambient

conditions in terms of pressure and temperature (i.e. p_{amb} and T_{amb}) that are passed to the refueling station and tank models. In the refueling station the user selects the hydrogen temperature at the tank inlet. In addition, if the PCM-tank is selected as the investigated system, the tank type (e.g. Type III or IV) and the initial pressure should also be given as inputs. These two parameters are used together with p_{amb} and T_{amb} to determine the appropriate refueling protocol, which, in turn, defines the fueling pressure ramp for CHG storage systems according to SAE J2601 as discussed in Ref. [7].

In the tank model all the equations concerning energy and mass balances, kinetics and heat transfer are solved (see Appendix B and Refs. [6], [7]). This occurs according to the model setup that the user defines. For the MHSS it is also possible to choose a variable parameter model in which the thermal conductivity and specific heat capacity are dependent upon pressure and hydrogen content, respectively, and are calculated by interpolating experimental data.

The user is required to participate into the model setup by defining values for the free variables (such as ambient temperature and pressure) and by selecting different options that are provided through some *if* –scenarios and libraries. The *if* –scenarios require that the user to decide whether a statement is *True* or *False* and then the program selects the appropriate set of equations and initial values to be used. For instance, if the user selects *True* for the *if* –scenario named "charging", then a charging analysis is going to be carried out. A discharging analysis is otherwise performed. In the same way, it is possible to decide the level of discretization for the MH bed domain (i.e. 0D or 1D).

The libraries give access to different heat exchanger configurations, metal hydride and phase change material compositions, boundary conditions, kinetic models and heat transfer media. A more detailed description of the libraries is given in Ref. [10]. If a specific choice is not taken, the nominal option for each database is selected by default according to the tables reported in the Appendix B. The nominal options are here used to obtain the results presented in the following sections.

2.1.1 Modeling tool

The platform has been designed in Dymola™ to take advantage of a robust environment for topological modeling with a non casual approach. The object-oriented language Modelica® offers the possibility to reuse packages and modeling knowledge via the hierarchical structure and inheritance constructs [11]. These aspects make Dymola™ a particularly convenient tool to develop robust exchangeable component libraries. The graphical user interface (GUI) allows customizing the component figures by either editing simple shapes or by uploading external picture files.

2.2 Tank design approach

The model implemented in HySDeP combines energy and mass balances as well as kinetic and heat transfer equations to estimate the time evolution of the solid bed temperature, hydrogen content, fueled hydrogen mass and transferred heat to/from the system. Details of the mathematical framework can be found in Ref. [6], [10], whereas the discretization model of the tubular bed is reported in Appendix A.

The design of the heat exchangers is based on the critical MH thickness (δ) concept defined as the distance from the cooling surface at which the hydrogen content reaches the target value at the desired refueling time [6].

In this study the hydrogen content is expressed by the fraction of reaction completion F_{rc} defined in Eq. 1 whereas the refueling time is set to 3 min.

$$F_{rc} = \frac{w}{w_{\max}} \cdot 100 \tag{1}$$

The fraction of reaction completion varies from 0% (fully dehydrided conditions) to 100% (fully hydrided conditions) and is solely function of the weight fraction of absorbed hydrogen in the hydride w (in $kg_{H2} \cdot kg_{MH}^{-1}$), whereas the saturation value w_{max} remains constant. The results presented in this study are obtained under the assumptions of completely reversible reactions and w is initialized with a zero-value to represent fully dehydrided conditions upon recharging. However, whenever trustable information from experimental investigations is available, the user can set a positive starting value for w to take into account irreversible absorbed hydrogen. For the absorbing alloy here considered, being $Ti_{1.1}CrMn$, w_{max} is equal to 1.5% [12].

In Fig. 2 F_{rc} is plotted against the refueling time at different locations (see the definition of dx in Appendix A) from the cooling surface under the nominal input values reported in Appendix B for the cooling and refueling conditions.

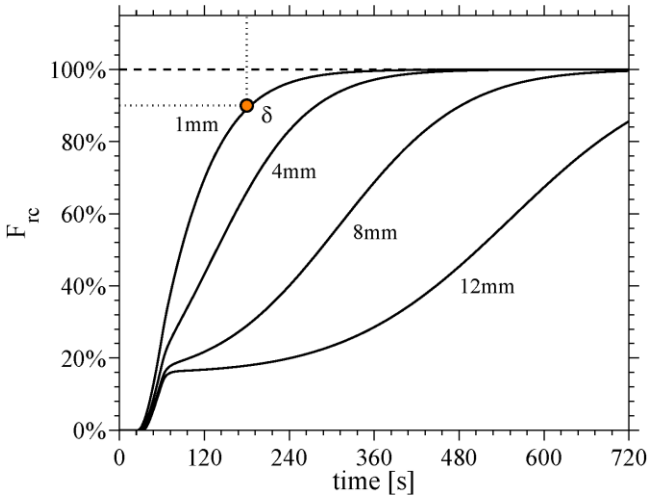

Fig. 2. Critical MH thickness for $Ti_{1.1}CrMn$ for target F_{rc} and refueling time of 90% and 3 min.

From Fig. 2 it can be seen that in order to achieve the F_{rc} and refueling time of interest, the thickness of the MH bed should never exceed 1 mm. Such a thickness represents half of the maximum distance comprised between two consecutive cooling elements for a solid bed geometry that is symmetric with respect to the direction of the heat transfer (see Ref. [6]).

As the selected absorbing alloy has a high dissociation pressure, the vessel containing the MH is here considered cylindrical to allow for a uniform distribution of the mechanical stresses that result from hydrogen pressurization. Under such a constraint, the vessel/heat-exchanger designs chosen for the analysis are based on the tubular tank design. The two configurations are here names as HEX1 and HEX2. In HEX1, the metal hydride is packed inside the inner tubes and the coolant flows parallel to the tube. This represents a tube-in-tube layout where the hydrogen-absorbing alloy occupies the volume in the inner tubes and the coolant flows in the annular region comprised between inner and outer tubes. In HEX2, the metal hydride is packed inside the tubes and the coolant circulates in the shell in a combined cross-parallel flow over the tube bank. These arrangements are shown in Fig. 3, whereas their thermal models can be found in Ref. [13].

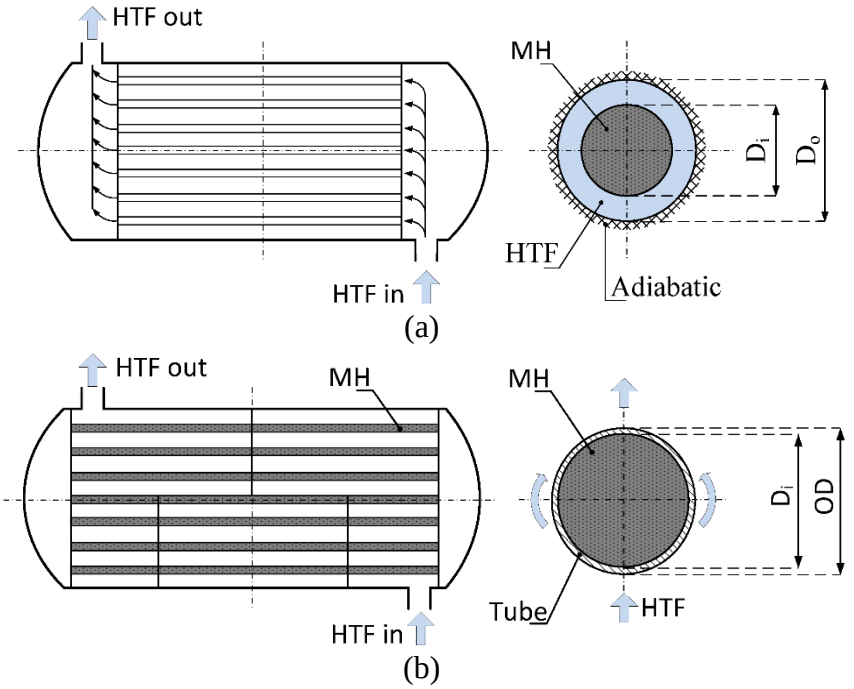

Fig. 3. Longitudinal system's section and tubes' transversal sections for: HEX1 with external adiabatic boundary (a) and HEX2 (b) [13].

According to the definition of δ, in order to achieve a uniform pattern of reaction and ensure that the solid bed will achieve the target absorbed hydrogen content by the desired fueling time at any location. The design of a tubular solid bed that follows the δ criterion provides several advantages over a chamber tank configuration.

Firstly, holding the metal hydride in tubes, rather than in a large-diameter vessel, eases the confinement and compaction of the hydrogen-absorbing alloy, which is hard to handle especially in the powder form. Additional advantages of such a configuration that are particularly important for high pressure MHSSs, include: reduced maintenance cost, increased heat transfer performance and uniformity of reaction in the solid bed. As the mechanical component that is dedicated to bear the high-pressure hydride is a metallic tube, the external container has the only function to provide the volume for the circulation of the low-pressure HTF and therefore, it can be constructed with a cheap plastic material. On the other hand, smaller thicknesses also imply smaller thermal resistance and reduced parasitic mass during heating/cooling. The confinement of the active alloy in small tubes promotes the realization of a uniform pattern of absorption/desorption, because it is easier to design the system according to the critical MH thickness criterion.

The tubular tank design with MH tubes is also attractive for its modularity which enables, in principle, to ease the maintenance of the system by replacing only the storage module that presents malfunctioning. A consequent reduction in the maintenance cost of the system is therefore expected. At the end, the storage tank can be a cheap plastic vessel with integrated thin metallic tubes that are easily obtainable in the market and serve the function of independent hydrogen-storage modules. Aluminum alloys (e.g. Al 6061-T6) and austenitic steels (e.g. AISI 304) typically present a good resistance to embrittlement [14], [15]. The main drawback of the tubular design is the reduced MH capacity when

compared to chamber-tank designs, as discussed in Ref. [16]. The mechanical and operative requirements for these designs were reported in Ref. [13].

2.2.1 Main input parameters for charging/discharging analyses

For the charging and discharging analyses the main inputs are listed in Table 1 and Table 2 respectively for HEX2. Besides the heat exchanger geometric parameters, the input data listed in these tables are also used to study the hydriding/dehydriding process for HEX1. For such a configuration, the results are obtained with an aspect ratio of 0.5 (see Ref. [13]).

Table 1. Model input parameters for charging analysis (HEX2).

Domain	Parameter	Value	Unit
amb.	p_{amb}	1.013	bar
	T_{amb}	20	°C
p_{ramp}	p_0	1.013	bar
	p_{ref}	300	bar
	duration	60	s
	time offset	0	s
cool.	Dexcool®		
	$\dot{m}_c$	20	$kg \cdot s^{-1}$
	$T_{c,in}$	0	°C
tank	L	1	m
	d_{tank}	0.4	m
MH	$Ti_{1.1}CrMn$		
	φ	60%	-
	δ	1	mm
tube	Al 6061-T6		
	OD	2.5	mm
HEX	HEX2		
	PR	1.25	-
	layout angle	30	deg
	baffle cut	25%	-
	baffle space	$50\% \cdot d_{tank}$	m

For the charging process the internal pressure of the tank is raised from the initial value, set equal to the ambient pressure, to the desired charging pressure of 300 bar in 1 minute. A coolant mass flow rate of 20 $kg \cdot s^{-1}$ flows through the heat exchanger and exchanges the heat of reaction with the solid bed inserted in tubes of 1 mm of radius and 1 m of length. The MH tubes are arranged in a bank with a pitch to tube diameter ratio *PR* of 1.25.

For the selected hydride ($Ti_{1.1}CrMn$) a large porosity value (60%) that corresponds to a packing density of 2500 $kg \cdot m^{-3}$ results from powder activation, which leads to small particles sizes with sharp edges. This value ensures a moderate compactness that diminishes the risk for further particle deformation during hydrogen absorption, but increases the contact resistance. In addition, such a high porosity value allows for hydride expansion with respect to an expected maximum volume increase by 23% during hydriding and therefore, the strain effects that result from MH swelling are assumed to be

compensated [12], [17]. For this reason, the mechanical stresses that the tubes can experience during hydriding/dehydriding cycles are neglected in the model.

Table 2. Model input parameters for discharging analysis (HEX2).

Domain	Parameter	Value	Unit
amb.	p_{amb}	1.013	bar
	T_{amb}	20	°C
p_{ramp}	p_0	300	bar
	p_{ref}	1.013	bar
	duration	600	s
	time offset	0	s
cool.	Dexcool®		
	$\dot{m}_c$	5	$kg \cdot s^{-1}$
	$T_{c,in}$	30	C
tank	L	1	m
	d_{tank}	0.4	m
MH	$Ti_{1.1}CrMn$		
	φ	60%	-
	δ	1	mm
tube	Al 6061-T6		
	OD	2.5	mm
HEX	Shell and tube		
	PR	1.25	-
	layout angle	30	deg
	baffle cut	25%	-
	baffle space	$50\% \cdot d_{tank}$	m

A fast dehydriding analysis is here investigated to study the ability of the system to fulfill intense discharging conditions. The internal pressure is lowered from the initial condition (i.e. 300 bar) to ambient pressure in 10 min. It is also assumed that any MHSS that can fulfill such conditions can also satisfy cyclic dehydriding characteristics, as it is typically required in real FCEVs operation.

From the Table 2 it should be observed that a much lower mass flowrate than in Table 1 is considered for the discharging process. This is done to take into account of the actual operation of the FCEV. In practice, the heating fluid is circulated in a closed loop inside the car and therefore, the mass flow rate is limited by the size of the heating system components (e.g. valves, tubes) and the cooling demand of the fuel cell. The heating fluid temperature at the inlet is set to 30 °C, which is the assumed value for the HTF that returns from the fuel cell system.

3. Results

This section focuses on the results obtained with HySDeP for charging and discharging processes in vehicular MH hydride storage tanks. The hydriding and dehydriding regions that correspond to the charging and discharging phases are shown for the absorbing alloy of interest in Fig. 4 where the equilibrium pressure for the absorption and desorption reactions are plotted against the bed's

temperature. For the absorption reaction to occur, the tank pressure must be above the equilibrium pressure identified by the upper black line (i.e. in the grey area), whereas the opposite is valid for the dehydriding reaction (i.e. blue area) with respect to the lower black line. It should be noticed that for any given temperature the equilibrium pressure is higher for the absorption process than the desorption reaction. For instance, at an ambient temperature of 20 °C, the equilibrium pressure is 160 bar for hydriding and 100 bar for dehydriding. Such a disparity in p^{eq} is due to the hysteresis phenomenon which results in a p-T region where neither absorption nor desorption can occur (white area comprised between the equilibrium pressure lines).

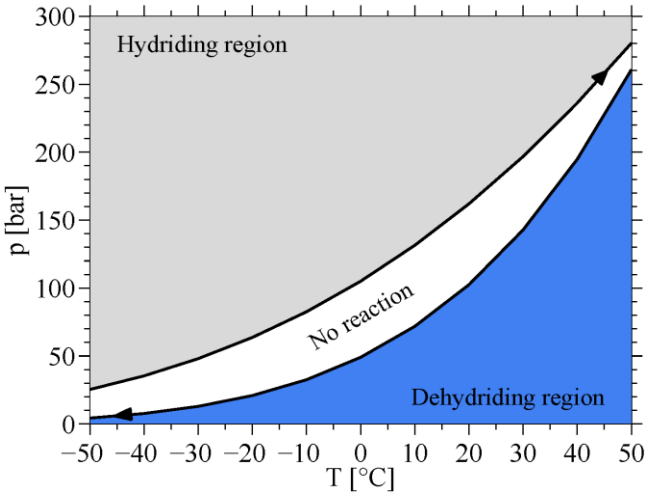

Figure 4. Hydriding and dehydriding regions for $Ti_{1.1}CrMn$.

The charging and discharging analyses are conducted for the two heat exchangers and a sensitivity analysis is carried out to address the effect of the main design parameters on the storage performance and system's weight. The results here presented refer to the discretization model described in Appendix A with a number of total discretization volumes of 5 for each MH tube and to the nominal input parameters identified in the methods section and in Appendix B, unless otherwise specified.

3.1. Charging analysis

The results of 0D and 1D fueling models are presented for the solid bed temperature, fraction of reaction completion and stored hydrogen mass for HEX2 in Fig. 5 and for HEX1 in Fig. 7. For both models and configurations the main inputs are listed in Table 1.

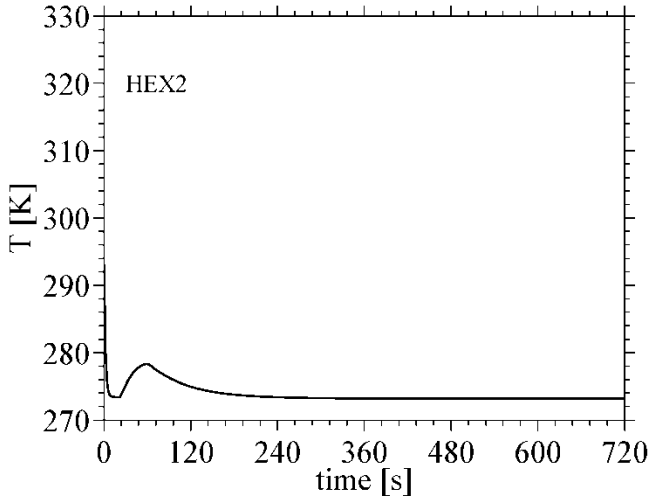
HEX2
T [K]
time [s]

(a)

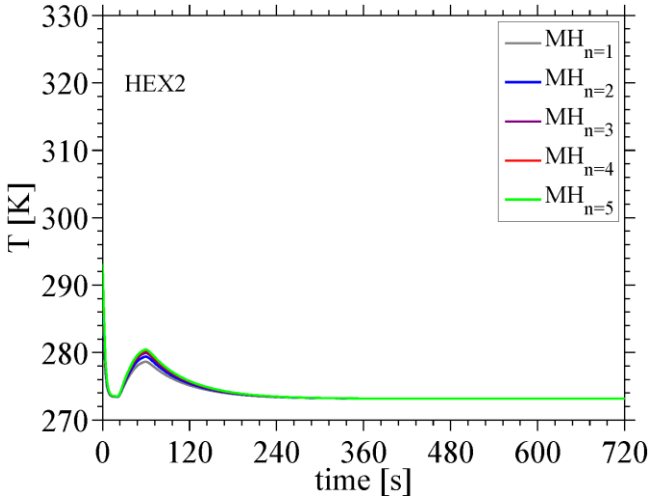
HEX2
T [K]
time [s]
MH n=1
MH n=2
MH n=3
MH n=4
MH n=5

(b)

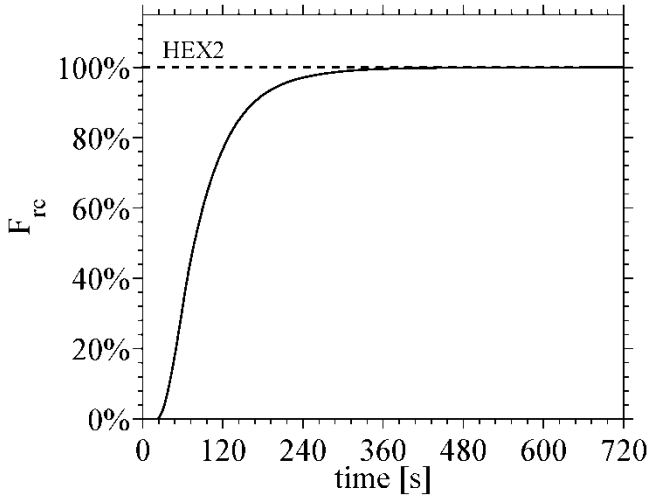
HEX2
F rc
time [s]

(c)

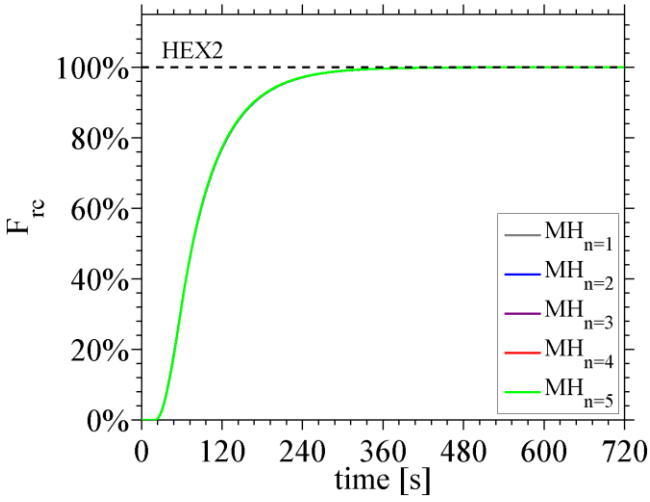
HEX2
F rc
time [s]
MH n=1
MH n=2
MH n=3
MH n=4
MH n=5

(d)

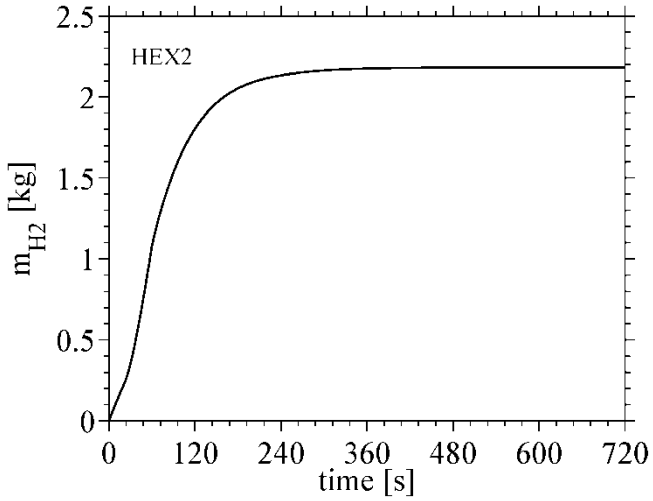
HEX2
m H2 [kg]
time [s]

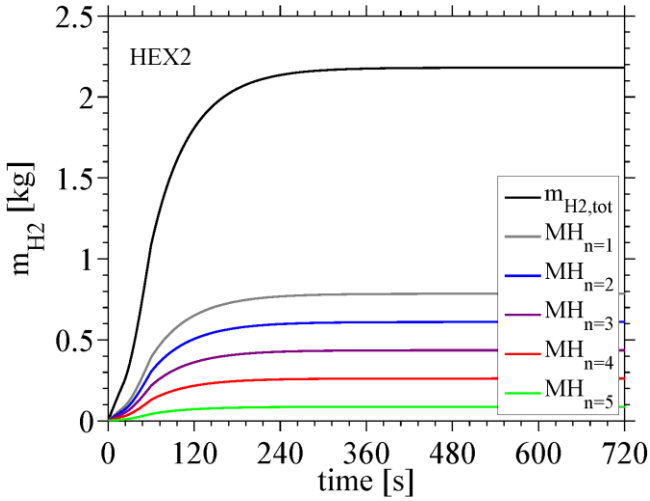
HEX2
m H2 [kg]
time [s]
m H2,tot
MH n=1
MH n=2
MH n=3
MH n=4
MH n=5

(e) (f)

Figure 5. Charging analysis: bed temperature for 0D (a) and 1D (b); fraction of reaction completion for 0D (c) and 1D (d); stored mass for 0D (e) and 1D (f). HEX2 layout.

From Fig. 5 it is possible to observe that the difference in results between the 0D and 1D model (with 5 MH concentric volumes) is negligible. This occurs because the investigated inner diameter (i.e. 2mm) is small enough that a lumped model is adequate to accurately describe the hydriding reaction within the solid bed. Figs. 5a-b show that the large cooling rates enable a rapid reduction in temperature, which drops from the initial conditions (i.e. 20 °C) to the coolant temperature before the absorption process takes place and then suddenly increases by 8 °C at the end of pressurization. Finally, the MH temperature tends to the coolant temperature reaching steady state conditions at 360 s.

Figs. 5c-d show the fraction of reaction completion for the 0D and 1D models. The small size of the MH tubes enable considerable bed cooling and therefore, significant hydriding rates. The small temperature differences between the concentric MH volumes have a negligible effect on the absorption rates, as the reaction is kinetically limited. As a result the F_{rc} curves are coincident in Fig. 5d. It is worth pointing out that the design achieves the desired F_{rc} of 90% within the target refueling time of 3 min.

Figs. 5e-f presents the total stored hydrogen mass which accounts for approximately 2.2 kg. In Fig. 5f the total fueled mass is obtained by adding the contributions of each concentric volume multiplied by the calculated number of tubes. Even though the hydrogen-absorbing alloy only occupies 40% of the bed volume (i.e. φ= 60%), c.a. 74% of the total fueled mass is stored in the absorbed phase and only 26% is stored in the gaseous form in the pores. This can be seen in Fig. 6.

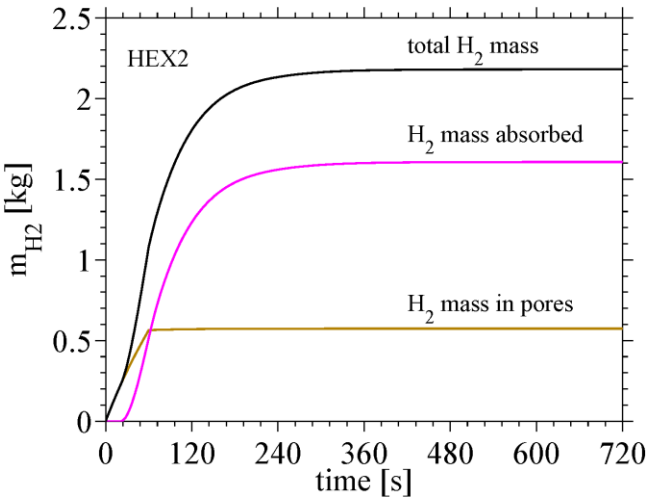

Figure 6. Hydrogen mass stored in the solid bed: mass in pores and in absorbed phase. HEX2 layout.

In Fig. 7 the 0D and 1D results for the bed temperature, fraction of reaction completion and stored mass are obtained for the HEX1 configuration with an aspect ratio of 0.5. From such a figure it can be observed that the difference in results between the lumped and spatially distributed models is negligible and the 0D model well describes the physical behavior of the storage system, as it was found for HEX2. The solid bed temperature profiles and the hydriding rates shown in Figs. 7a-b and in Figs. 7c-d are nearly coincident with those obtained for HEX2, even though the convection coefficient of heat

transfer for HEX1 (i.e. 1500 $W \cdot m^{-2} \cdot K^{-1}$) is less than half than for HEX2 (i.e. 3420 $W \cdot m^{-2} \cdot K^{-1}$) under the same cooling conditions. This occurs because the heat transfer process is dominated by the conductive thermal resistance of the metal hydride. Although the cooling performance and hydriding rates are comparable for HEX1 and HEX2, it is possible to notice that the former configuration stores a much lower hydrogen mass (Fig. 7e-f). The reason for this lies in the disparity of the MH volume, which occupies only 8.5% of the total inner tank volume for HEX1 and 34.7% for HEX2. As a result, HEX2 enables storing 4 times more stored hydrogen mass than HEX1. In order to maximize the hydrogen stored mass, its dependency upon the main geometric parameters is investigated in the parametric analysis section.

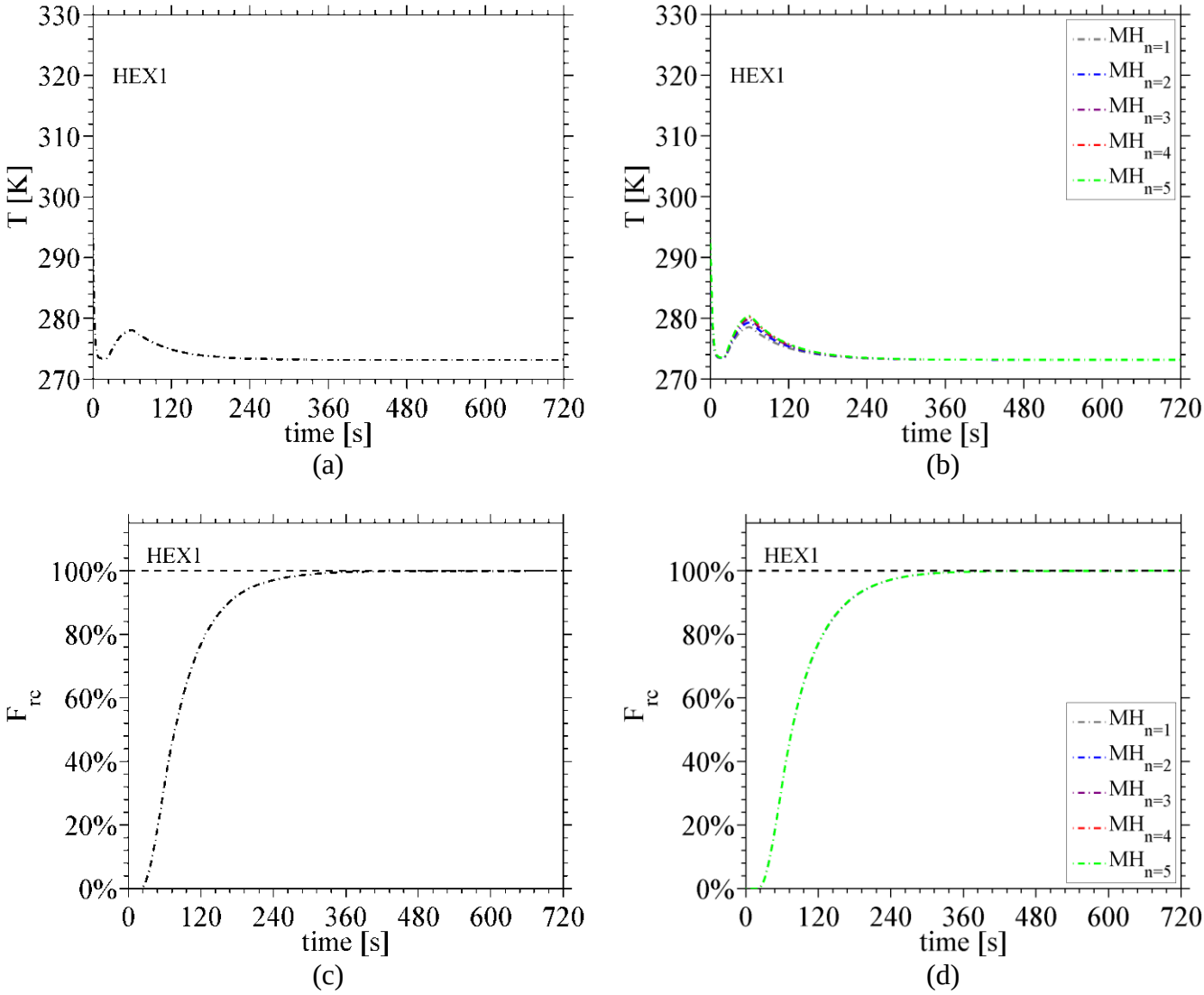

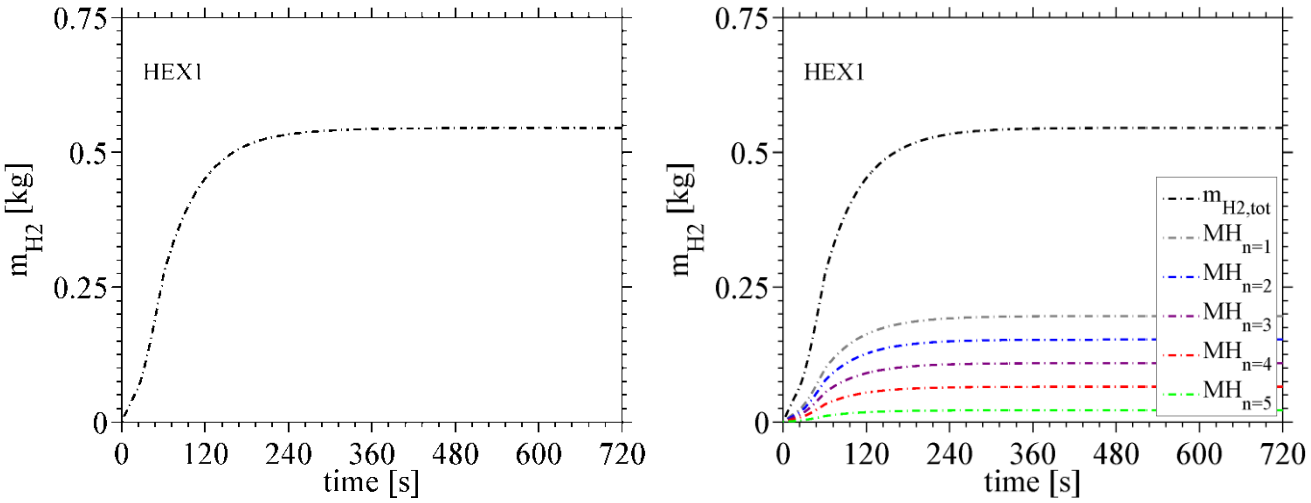

Figure 7. Charging analysis: bed temperature for 0D (a) and 1D (b); fraction of reaction completion for 0D (c) and 1D (d); stored mass for 0D (e) and 1D (f). HEX1 layout.

Results similar to those presented in Figs. 5 and 7 can be obtained for coolant rates much lower than the chosen value of 20 kg·s^{-1} that is here selected to operate at a shell-side velocity value (i.e. 1.17 m·s^{-1}) comprised between the minimum and maximum recommended values to reduce the risk of deposits and prevent the tube corrosion [13]. In addition, from Fig. 8 it can be noticed that such a flow rate provides a maximum difference of only 2 °C between inlet and outlet temperatures. This confirms the assumption of constant cooling conditions over the entire length of the heat exchanger that is typically considered in practice for MHSSs. Differently, caution in using this assumption should be taken when very low coolant rates are considered (i.e. below 15 kg·s^{-1}).

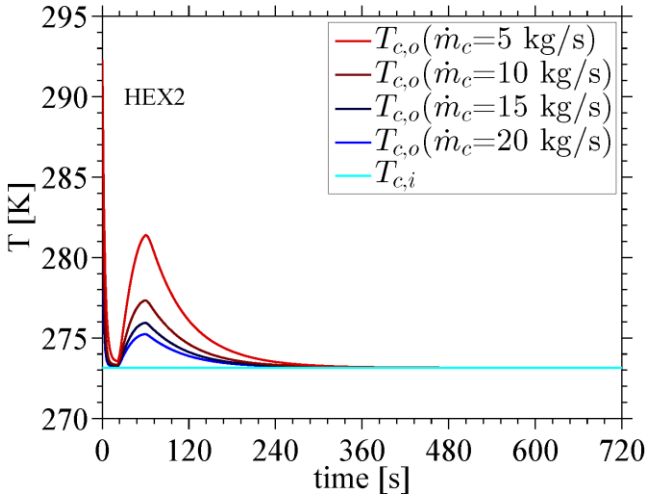

Figure 8. Inlet and outlet coolant temperatures. HEX2 configuration.

3.2. Discharging analysis

Simulations show that, as it was found for hydrogen absorption, the difference in results between the 0D and 1D models is negligible for the desorption process. Therefore, the results of the discharging analysis are presented with respect to the 0D model to ease the reading of the plots. Fig. 9 shows the results obtained for the bed temperature, fraction of reaction completion and desorbed hydrogen mass for both HEX2 and HEX1 configurations. In Fig. 9a it is possible to notice that the metal hydride temperature rises sharply from the initial conditions to the heating fluid inlet temperature of 30 °C and then remains constant until the tank pressure decreases below the equilibrium pressure triggering the hydrogen desorption at approximately 312 s. The endothermic nature of the reaction causes the solid bed to suddenly cool down, reaching similar minima for the two configurations in a specular way of what observed for the hydriding process.

Further, the heat absorbed to maintain desorption reaction increases the metal hydride temperature back to the inlet HTF temperature. Fig. 9b shows that the two heat exchanger configurations provide nearly coincident profiles for the fraction of reaction completion. The reaction is kinetically-limited and the temperature decrease observed in Fig. 9a has only a negligible effect on the dehydriding rates.

In Fig. 9c the stored mass decreases at first for the effect of the decreasing pressure until the dehydriding reaction is triggered. A considerable mass leaves the tank between 312 s and 456 s when the reaction is completed. From this moment only the hydrogen mass in the pores continues to decrease until the valve closes at 600 s and the system reaches stationary conditions. The total desorbed hydrogen mass shows significantly different values for the two configurations, because of the different storage volumes realized by the two configurations. It can be observed that, for both configurations, the initial mass differ from the values reached at the end of the charging process in Figs. 5e-f and Figs. 7e-f. This is mainly due to the difference in the starting and final conditions set for F_{rc} in the two processes (i.e. 90% and 100% for hydriding and dehydriding respectively) and in minor part to the different temperatures, thus densities, of the hydrogen in the gas phase. At the end, both configurations enable fast discharging under practical heating conditions. The difference in the dehydriding performance is negligible for HEX1 and HEX2 and the only considerable disparity lies in the storage volume of the two layouts and thus, in the total hydrogen mass available to operate the FCEV.

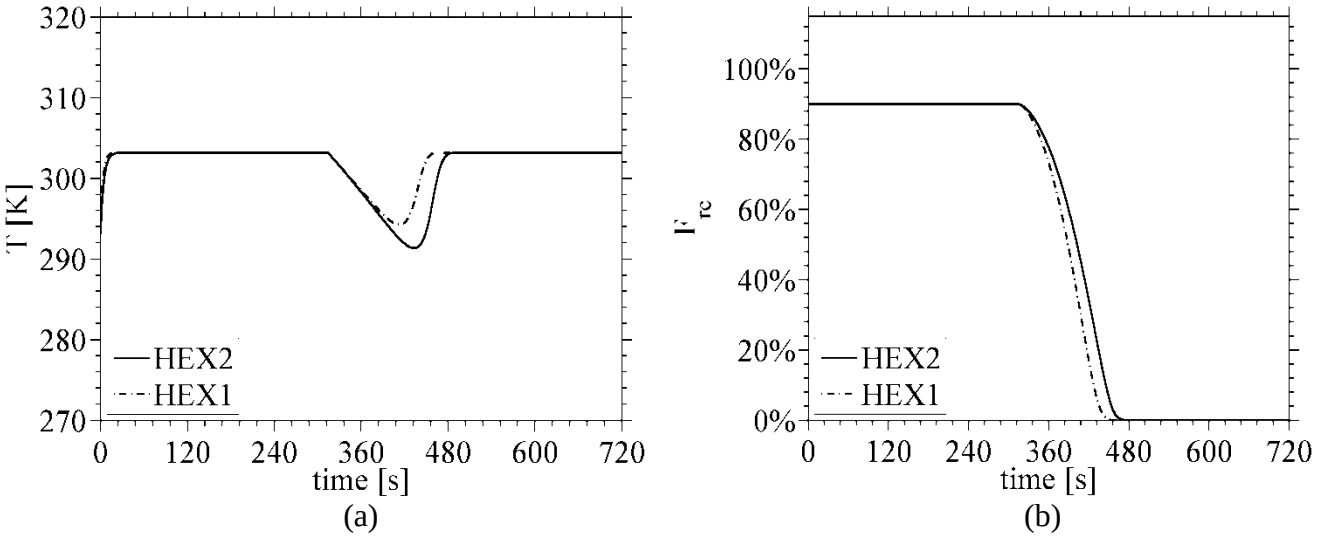

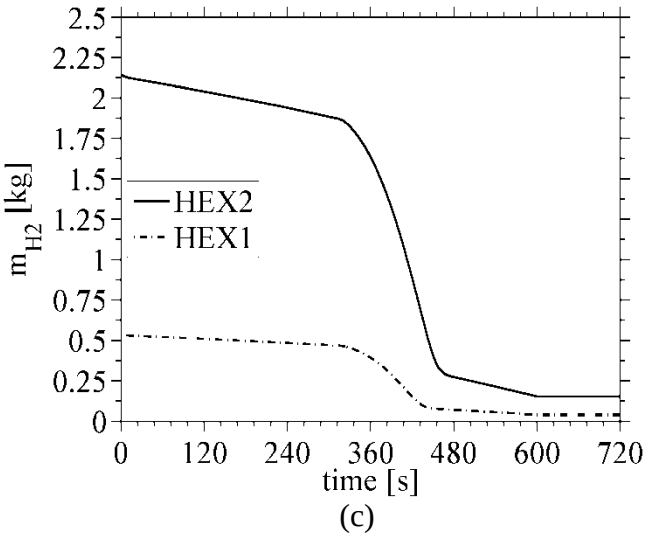

Figure 9. Discharging analysis: bed temperature (a); fraction of reaction completion (b); stored mass (c). HEX3 and HEX2 configurations.

3.3. Parametric analysis

The charging and discharging analyses showed that the drawback of the investigated designs is the small MH volume available for hydrogen storage. Therefore, in this section a sensitivity study on the main geometric parameters is carried out with the aim of optimizing the overall stored hydrogen mass. The results here reported refer to the input data listed in Table 1. It is worth pointing out that the inner diameter is not varied here as its value is the result of a design analysis based upon the critical MH thickness that achieves the target F_{rc} and the desired refueling time. According to the thermal model described in Ref. [13] the only design parameters that influence the hydrogen stored mass are the pitch to tube diameter ratio *PR* for HEX2 and the aspect ratio *a* for HEX1. The latter is expressed as the ratio of D_i to D_o with respect to Fig. 3a.

Fig. 10 shows the dependency of the hydrogen mass upon the pitch to tube diameter ratio *PR* for HEX2 on the left y-axis. The corresponding ratio (i.e. V_{ratio}) is between the MH volume and the inner tank volume plotted on the right y-axis.

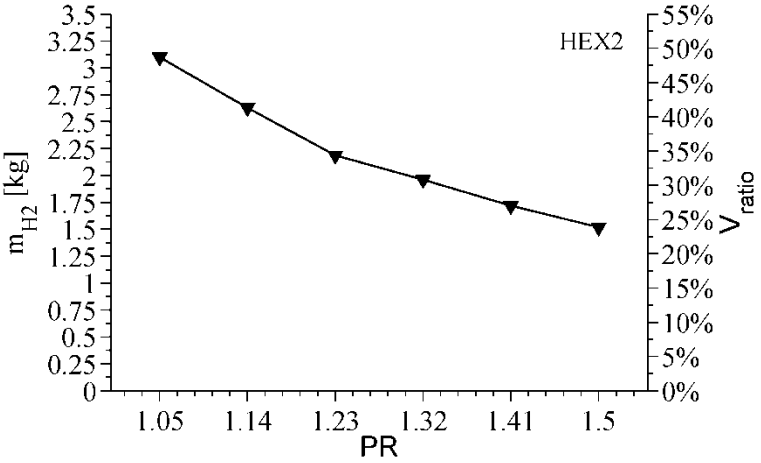

Figure 10. Stored hydrogen mass and volume ratio as functions of pitch to tube diameter ratio (HEX2).

A decrease in the *PR* value corresponds to a reduced distance between the tubes and therefore to an increase number of MH tubes inside the tank. A maximum value of 3.09 kg is achieved for a pitch to tube diameter ratio of 1.05 and V_{ratio} becomes 48.7%. However, it is worth mentioning that practical PR values typically do not fall below 1.25 to avoid the weakening of the tube sheet [18]. In addition, as the storage capacity is enlarged by increasing the MH volume, the stored hydrogen mass increases with the absorbing alloy's weight resulting in a larger volumetric density and a constant gravimetric density, which settles at 1.25%. This can be seen in Fig. 11 where the weight of the tank is shown for a pitch to tube diameter ratio of 1.05 and for its nominal value. The volumetric density increases from 0.0173 to 0.0246 kg_{H2}/L_{syst}. The increase in the volumetric density that occurs at lower pitch to tube diameter ratio values is compensated by the larger storage system's weight, which varies from 175 kg to 250 kg in the *PR* range of 1.25-1.05. In both cases the heaviest tank component is the absorbing alloy, which accounts for more than 61% of the total tank's weight, followed by the heat exchanger, i.e. 37.5% (Al6061-T6 tubes), and hydrogen 1.25%.

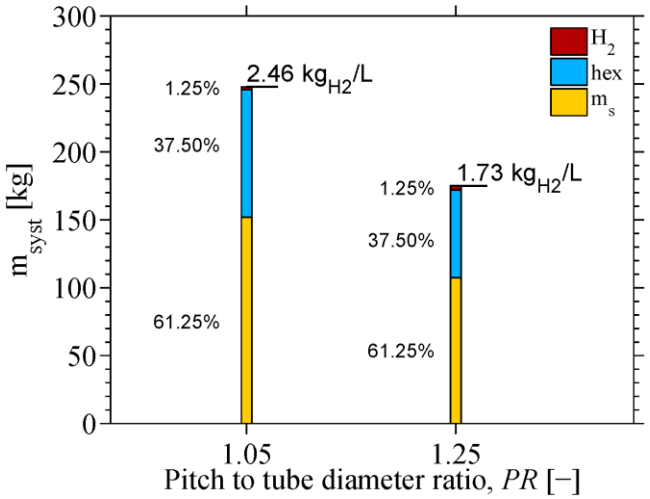

Figure 11. Weight of the main tank's components: hydrogen, heat exchanger and absorbing alloy (HEX2).

Fig. 12 shows the dependency of the hydrogen mass upon the aspect ratio for HEX1 on the left y-axis. The respective V_{ratio} is plotted on the right y-axis. For HEX1, increasing the aspect ratio at constant inner diameter corresponds to reducing the outer tube inner diameter (see Ref. [13]) and therefore increasing the available volume for MH tubes. The stored hydrogen mass (and the MH volume) increase exponentially with the aspect ratio, as the number of tubes has an exponential dependency upon the outer diameter [19]. However, reducing the outer tube diameter means that the cross flow area for the heat transfer fluid decreases with *a*. As a result, one could expect that decreasing the HTF mass flow rate would cause a reduction in the cooling performance. Simulations have shown that for an inner diameter of 2 mm and an aspect ratio of 0.9 the minimum mass flow rate that enables achieving the target F_{rc} at the desired time of 3 min is 0.5 kg·s^{-1}. Finally, although the stored hydrogen mass significantly increases when the aspect ratio varies from 0.1 to 0.9, the maximum m_{H2} (i.e. 1.77 kg) is comparable with the minimum value obtained with a *PR* of 1.5 for HEX2 (i.e. 1.51 kg).

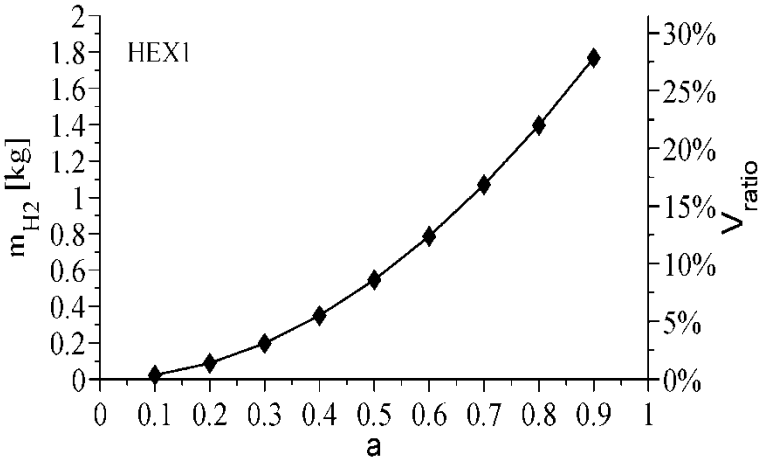

Figure 12. Stored hydrogen mass and volume ratio as functions of aspect ratio (a).

4. Conclusion

A modeling platform is successfully developed in the Dymola™ environment to design and simulate on-board hydrogen storage systems. At the moment of the submission of the present study HySDeP includes a MH storage system model based on tubular tank layout and a CHG storage system with a standard and a novel design with integrated PCM.

The computational platform is built with attention to the key design criteria of user friendliness, flexibility and facility of third party development. The main structures (or classes in the Modelica® language) are divided in macro and sub-models, records, ports and functions. The architecture is kept simple and the models are grouped in modeling packages by category.

HySDeP can be used to perform both charging and discharging analyses. Examples of both are discussed in the present work for the MHSS and a comparison between the storage and cooling performance of two tank/heat-exchanger configurations, based on the tubular bed design, is provided.
The heat exchangers refer to a tube-in-tube and shell-and-tube layouts named HEX1 and HEX2 respectively. The MH is placed in tubes of 2 mm of inner diameter in order to achieve the targets for F_{rc} (i.e. 90%) and refueling time (i.e. 3 min). If a sintered filter is introduced in the tube to enable

hydrogen distribution within the solid bed, the tube size should be enlarged in practice to account for the filter diameter. However, as the filter would be inserted at the adiabatic center-line of the tube, its mass would not affect the heat transfer and therefore, it has been neglected in this study.

For both the HEX2 and HEX1 layouts the 0D and 1D models provide equivalent results and well describe the reactions that occur within the solid bed. The small tube size enables efficient heat transfer over the entire MH thickness and thus considerable significant hydriding rates. As a result, the reaction is kinetically limited and the temperature increase that occurs during hydrogen absorption is not sufficient to slow down the reaction.

Although the two heat exchanger configurations realize similar cooling and kinetic performance, a great disparity occurs for the amount of stored hydrogen mass. This is due to the difference in the MH volume available for hydrogen storage. HEX2 achieves a total hydrogen mass of nearly 2.2 kg, whereas HEX1 is able to store approximately one fourth of this value. Such a mass is stored mainly in the absorbed phase (c.a. 74% of the total fueled mass), even though the hydrogen-absorbing alloy occupies only 40% of the bed volume (i.e. φ= 60%). The same results can be obtained under the assumption of constant HTF temperature between inlet and outlet, as for practical flow rates the thermal gradient in the fluid flow can be neglected.

The discharging analysis reveals that both HEX2 and HEX1 enable fast dehydriding under practical heating conditions. As it was found for the charging process, the two layouts provide similar heat-transfer and kinetic performance and the only considerable difference lies in the amount of hydrogen that is available to operate the FCEV. To overcome this issue a sensitivity analysis is carried out with respect to the main geometric parameters for each configuration to maximize the hydrogen stored mass. For HEX1 increasing the aspect ratio provides significant hydrogen mass augmentation, which varies between 0.02 kg to 1.77 kg in the range of 0.1-0.9 for *a*. However, even in the most favorable conditions, the total stored mass is slightly larger than the minimum value realized for HEX2 (1.51 kg), which occurs for a pitch to tube diameter ratio, *PR*, of 1.5. Decreasing *PR* allows packing more MH tubes in a fixed volume and thus, storing a larger hydrogen mass, which reaches 3.1 kg for a pitch to tube diameter ratio of 1.05. However, the increase in the volumetric density (from 0.0173 to 0.0246 kg_{H2}/L_{syst}) is compensated by the larger storage system's weight, which varies from 175 kg to 250 kg for a *PR* between 1.25 to 1.05. In both cases the heaviest tank component is the absorbing alloy, which accounts for more than 61% of the total tank's weight, followed by the heat exchanger, i.e. 37.5% (Al6061-T6 tubes), and hydrogen 1.25%. As a result the gravimetric storage capacity is found to be independent from *PR* with a constant value of 1.25%.

Finally, in order to overcome the limitations on volumetric and gravimetric storage capacities of MHSSs, further research on both tank design and light-weight absorbing alloys is necessary.

Acknowledgements

The authors acknowledge the Danish Energy Agency for financial support, our industrial partner H2Logic, and all of the members of the Hyfill-Fast International Research Project for their collaboration.

Appendix A. Heat exchanger design models for the MHSS

The tubular domain under investigation and the concentric discretized MH volumes *n* are shown in Fig. A.1 together with the longitudinal and radial discretization steps, i.e. *dl* and *dx* respectively. The latter parameter is calculated once the inner diameter D_i and the number of discretized volumes *N* (i.e.

4 in the figure) are set by the user. On the other hand, *dl* is computed with respect to the tube length and a constant number for the coolant volumes *S*.

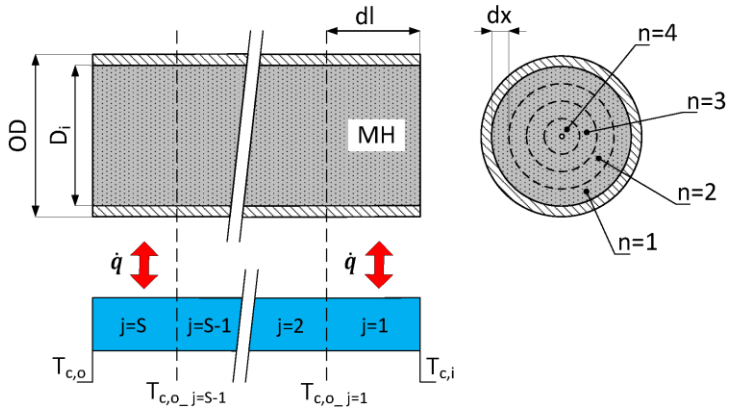

Figure A.1. MH tubular domain and discretization details.

A large number of discretization volumes is not necessary for the coolant domain, as the relatively large mass flow rates make the temperature gradient between inlet and outlet typically negligible. Each tube is treated as a separate heat transfer module that transfers the heat to the coolant. The total transferred heat is calculated by multiplying the single contributions by the maximum number of tubes that fit in the tank volume (see Ref. [13]). The heat is radially exchanged between the heat transfer fluid and the MH in the bed and it is used to calculate the HTF outlet temperature for each HTF volume based on a central differential scheme. As the heat transfer takes place radially, the center of the tube is an adiabatic surface.

When the shell and tube configuration is selected, it is possible to choose either the Bell-Delaware or Kern methods to calculate the convection coefficient (h_c) of heat transfer and the pressure drops. Even though the former provides a higher precision in the calculation of h_c, it requires the detailed definition of the heat exchanger geometry, which is not typically available in a pre-design stage. In such cases, it might be better to use the Kern method, which gives a good approximation of the value h_c in an early stage of design.

Appendix B. HysDeP: user libraries for the MHSS

The record structure in Modelica® language is used in HySDeP to create databases for material properties, geometric parameters and to select among different boundary conditions and kinetics equations. Each database is defined by a name (e.g. *MH_properties*, *Tube_properties*) and a variable number of fields that characterize data using types such as *Real* or *Integer* for numbers and *Boolean* for logic parameters. The underlined text that appears in the tables of this appendix corresponds to the default entries that the platform selects unless a selection is made by the user. As an example, if no hydrogen-absorbing alloy is chosen, the model uses the properties of $Ti_{1.1}CrMn$, which is the nominal composition. The current appendix presents the status of the implemented libraries for the MHSS at the moment of the submission of this work. The user libraries that refer to the CHG system (e.g. PCM compositions) can be found in Ref. [10].

MH composition database

The results presented in this thesis for the MH tank refer to the nominal composition presented in for $Ti_{1.1}CrMn$. As it was mentioned in the methodology section other hydrogen-absorbing alloys can be selected from the user. The current status of the implemented materials is listed in Tables B.1 along with the relevant thermo-physical for hydriding and dehydriding processes, whereas the kinetic properties can be found in Ref. [10]. These materials represent the first effort of building a comprehensive library for those alloys for which kinetic and thermal properties are available in literature. All the listed materials can only be used in the constant parameter model, with the exclusion of $Ti_{1.1}CrMn$, for which, measured data has been implemented for thermal conductivity and specific heat capacity [6].

Table B.1. Metal hydride compositions and thermal properties included in HySDeP.

Composition	$\mathbf{k_{MH}}$ **[**$W \cdot m^{-2} \cdot K^{-1}$**]**	$\mathbf{c_{MH}}$ **[**$J \cdot kg^{-1} \cdot K^{-1}$**]**	$\mathbf{\rho_s}$ **[**$kg \cdot m^{-3}$**]**
$Ti_{1.1}CrMn$ [12]	1	500	6200
$Ti_{1.1}CrMn$* [20]	10	500	6200
$TiFe_{0.8}Ni_{0.15}V_{0.05}$ [21], [22]	1	500	6600
$Ti_{0.95}Zr_{0.05}CrMn$ [21], [23], [24]	1	500	6600
$LaNi_5$ [25], [26]	1.2	419	8200
$LaNi_{4.95}Sn_{0.05}$ [21], [22]	1	500	7200
$LaNi_{4.7}Al_{0.3}$ [27], [28]	5	419	8000

*compacted with Al powder.

Heat exchanger database

Table B.2 presents the configurations implemented in the heat exchanger library. These designs refer to the geometric layouts of Fig. 3.

Table B.2. Configurations implemented in the heat exchanger library.

Type	**Name**	**Description**
Tube-in-tube	HEX1	Bank of coaxial cylindrical tubes. Metal hydride inside the inner tube. HTF in the annular region.
Shell-and-tube	HEX2	Bank of bear tubes. Metal hydride inside the tube. HTF in the shell.

Heat transfer media database

With the only exception of the nominal heat transfer medium, Dexcool®, the properties for the other media are retrieved from Coolprop at a fixed pressure of 1 bar and at the calculated average temperature between inlet and outlet. The list of the available compositions is given in Ref. [29].
The properties of Dexcool® are given in Ref. [12] for the constant temperature of 0 °C.

Kinetic model database

Charging and discharging kinetic models other than the nominal equations presented in Ref. [6] can be selected from the user according to the chosen MH composition. The kinetic equation can be considered as a combination of three separate functions: the Arrhenius constant which is only function of the MH temperature, a pressure limiting function a composition function which depends on reaction order. This is shown in Eq. B.1:

$$\frac{\partial w}{\partial t} = C_a e^{E_a/(RT_{MH})} \cdot f_p(p, p^{eq}) \cdot f_w(w, w_{\max}, p, p^{eq}) \tag{B.1}$$

where C_a is the activation rate E_a is the energy of activation, R is the universal gas constant, p is the tank pressure and p^{eq} is the equilibrium pressure. Specifying the kinetic model means providing the properties of the hydrogen-absorbing alloy and selecting the pressure and composition functions. Table B.3 presents some typical expressions of f_p and f_w, used for modeling that are implemented in the database.

Table B.3. Pressure and composition functions included in HySDeP [21], [30].

Type	f_w	f_p	**Type**
0^{th} order abs.	w_{max}	$(p-p^{eq})/p^{eq}$	Normalized
0^{th} order des.	w_{max}	$\ln(p/p^{eq})$	Logarithmic
1^{st} order abs.	$(w_{max} - w)$ or $(1 - F_{rc})$		
1^{st} order des.	w *or* F_{rc}		

Finally it is worth pointing out that the composition function can be written for w or F_{rc}, depending on the variable that appears in the partial derivative on the left hand side of equation B.1.

Tube material database

Table B.4 presents the list of materials available in the *Tube_properties* library. Considerations on the operative pressure, rather than on the thermal properties, should be done when selecting these materials. Therefore, the library also includes the relevant mechanical properties (i.e. ultimate tensile strength and tensile yield strength) that are needed to calculate the minimum thickness that can bear the operative pressure of choice (see Ref. [31]).

Table B.4. Tube materials properties included in the HySDeP [15], [31].

Material	**Type**	**k** **[W·m^{-2}·K^{-1}]**	**c** **[J·kg^{-1}·K^{-1}]**	**ρ** **[kg·m^{-3}]**	**σ_y** **[MPa]**	**σ_u** **[MPa]**
Aluminum 6061 T-6	Aluminum alloy	167	896	2700	276	310
Aluminum 6351 T-6	Aluminum alloy	176	890	2710	283	310
Aluminum 6063	Aluminum alloy	200	900	2700	214	241

T-6						
Aisi 304	Austenitic Cr-Ni stainless steel	16.2	500	8000	215	505
Aisi 302	Austenitic Cr-Ni stainless steel	16.2	500	7860	275	620
Aisi 316	Austenitic Mo stainless steel	16.3	500	8000	290	580
Copper	Copper	398	385	8930	33.3	210

Nomenclature

a	aspect ratio for the tube-in-tube layout
C_a	activation rate, s^{-1} R is the universal gas constant
c	specific heat capacity, $J \cdot kg^{-1} \cdot K^{-1}$
D_i	inner diameter of the inner tube, m or mm
D_o	inner diameter of the outer tube, m or mm
dl	longitudinal discretization step
d_{tank}	inner diameter of the vessel, m
dx	radial discretization step
E_a	activation energy, $J \cdot mol^{-1}$
F_{rc}	fraction of reaction completion, $kg_{H2} \cdot kg_{MH}^{-1}$ or %
f_p	pressure limiting function, Pa
f_w	reaction rate function
k	thermal conductivity, $W \cdot m^{-2} \cdot K^{-1}$
L	active tube length, m
m	mass, kg
$\dot{m}_c$	coolant mass flow rate, $kg \cdot s^{-1}$
N	number of volumes used to discretize the metal hydride domain
n	discrete index of the metal hydride volumes
OD	outer diameter of the inner tube, m or mm
p	pressure, bar
p^{eq}	Equilibrium pressure, Pa
p_{ramp}	pressure ramp, bar/min
p_0	initial tank pressure, bar
S	number of volumes used to discretize the coolant domain
T	temperature, °C or K
V_{ratio}	ratio between the MH volume for all tubes and the inner tank volume

Greek symbols

δ	critical metal hydride thickness, m or mm
ρ	density, $kg \cdot m^{-3}$
φ	Porosity of the hydride bed, $m_{H2}^3 \cdot m_{MH}^{-3}$ or %

Subscripts

abs.	absorption reaction
c	coolant
des.	Desorption reaction
i	inlet
j	discrete index of the coolant volumes
o	outlet
ref	refueling
s	crystalline solid
syst	system

Abbreviations

amb.	ambient
CHG	compressed hydrogen gas
cool.	coolant
FCEV	fuel cell electric vehicle
GUI	graphic user interface
HEX	heat exchanger
MH	metal hydride
MHSS	metal hydride storage system
PCM	phase change material
PR	pitch to tube diameter ratio

References

[1] K. Edenhofer, O. R. Pichs-Madruga, Y. Sokona, E. Farahani, S. Kadner, T. Z. and J. C. Seyboth, A. Adler, I. Baum, S. Brunner, P. Eickemeier, B. Kriemann, J. Savolainen, S. Schlömer, C. von Stechow, and Minx, "Climate Change 2014: Mitigation of Climate Change. Contribution of Working Group III to the Fifth Assessment Report of the Intergovernmental Panel on Climate Change," *Cambridge Univ. Press. Cambridge, United Kingdom New York, NY, USA*, p. 2014, 2014.

[2] A. Yamashita, M. Kondo, S. Goto, and N. Ogami, "Development of high-pressure hydrogen storage system for the toyota mirai.," *Tech. report, SAE Tech. Pap.*, 2015.

[3] Toyota Motor Corp., "Toyota mirai. A turning point from the inside out." Available at: https://ssl.toyota.com/mirai/fcv.html. [Accessed: 11 Nov.-2016].

[4] T. Riis, E.F. Hagen, P.J.S. Vie, and Ø Ulleberg, "Hydrogen production and storage–r&d priorities and gaps." International Energy Agency-Hydrogen Co- Ordination Group-Hydrogen Implementation Agreement, 2006.

[5] D. Mori and K. Hirose, "Recent challenges of hydrogen storage technologies for fuel cell vehicles," *Int. J. Hydrogen Energy*, vol. 34, no. 10, pp. 4569–4574, May 2009.

[6] A. Mazzucco and M. Rokni, "Generalized computational model for high- pressure metal hydrides with variable thermal properties," *Int. J. Hydrogen Energy*, vol. 40, no. 35, pp. 11470–11477, 2015.

[7] A. Mazzucco, E. Rothuizen, J. Jørgensen, T. R. Jensen, and M. Rokni, "Integration of phase

change materials in compressed hydrogen gas systems : Modelling and parametric analysis," *Int. J. Hydrogen Energy*, vol. 41, no. 2, pp. 1060–1073, 2016.

[8] E. D. Rothuizen, "Hydrogen fuelling stations: a thermodynamic analysis of fuelling hydrogen vehicles for personal transportation". PhD Thesis (Technical University of Denmark), ISBN: 978-87-7475-371-1.

[9] A. Mazzucco, "HySDeP: Hydrogen Storage and Design Platform," 2016. [Online]. Available: https://github.com/DTU-TES/HySDeP_Hydrogen-Storage-Design-Platform. [Accessed: 08-May-2016].

[10] A. Mazzucco, "Tank designs for combined high pressure gas and solid state hydrogen storage" Technical University of Denmark. PhD Thesis (Technical University of Denmark), ISBN: 978-87-7475-443-5.

[11] P. Fritzson, *Principles of object-oriented modeling and simulation with Modelica 2.1*. John Wiley & Sons, 2010. ISBN 0-471-471631.

[12] M. Visaria, I. Mudawar, T. Pourpoint, and S. Kumar, "Study of heat transfer and kinetics parameters influencing the design of heat exchangers for hydrogen storage in high-pressure metal hydrides," *Int. J. Heat Mass Transf.*, vol. 53, no. 9–10, pp. 2229–2239, Apr. 2010.

[13] A. Mazzucco, T. G. Voskuilen, E. L. Waters, T. L. Pourpoint, and M. Rokni, "Heat exchanger selection and design analyses for metal hydride heat pump systems," *J. Hydrog. Energy*, vol. 41, pp. 4198–4213, 2016.

[14] M. R. Louthan, G. R. Caskey, J. A. Donovan, and D. E. Rawl, "Hydrogen embrittlement ofmetals.," *Mater. Sci. Eng.*, vol. 10, pp. 357–368, 1972.

[15] L. Klebanoff, "Hydrogen storage technology: materials and applications". CRC Press, 2012. ISBN: 978-1-4398-4107-5.

[16] A. Mazzucco, M. Dornheim, M. Sloth, T. R. Jensen, J. O. Jensen, and M. Rokni, "Bed geometries, fueling strategies and optimization of heat exchanger designs in metal hydride storage systems for automotive applications: A review," *Int. J. Hydrogen Energy*, vol. 39, no. 30, pp. 17054–17074, Oct. 2014.

[17] K. C. Smith and T. S. Fisher, "Models for metal hydride particle shape, packing, and heat transfer," *Int. J. Hydrogen Energy*, vol. 37, no. 18, pp. 13417–13428, 2012.

[18] Tubular Exchanger Manufacturers Association (TEMA). "*Standards of the Tubular Exchanger Manufacturers Association*" Inc., Tarrytown, New York (2007).

[19] S. Kakaç and H. Liu, "*Heat exchangers: selection, rating, and thermal design"*, 3rd ed. CRC Press, 2010. ISBN: 978-1-4398-4990-3.

[20] M. Raju, J. P. Ortmann, and S. Kumar, "System simulation model for high-pressure metal hydride hydrogen storage systems," *Int. J. Hydrogen Energy*, vol. 35, no. 16, pp. 8742–8754, Aug. 2010.

[21] T. G. Voskuilen, E. L. Waters, and T. L. Pourpoint, "A comprehensive approach for alloy selection in metal hydride thermal systems," *Int. J. Hydrogen Energy*, vol. 39, no. 25, pp. 13240–13254, Aug. 2014.

[22] T. Voskuilen and L. E. Waters, “Purdue metal hydride toolbox". Available at: http://github.com/PurdueH2Lab/MetalHydrideToolbox”. [Accessed: 12-Dec-2015].

[23] J. P. Vanhanen, P. D. Lund, and M. T. Hagstrom, “AB2 metal hydrides for high-pressure and narrow temperature interval applications,” *J. Alloys Compd.*, vol. 269, pp. 288–293, 1998.

[24] J.P. Vanhanen, P.D. Lund and M.T. Hagstrom, “Combined hydrogen compressing and heat transforming through metal hydrides,” *J. Hydrog. Energy*, vol. 24, pp. 330–337, 1999.

[25] F. Laurencelle and J. Goyette, “Simulation of heat transfer in a metal hydride reactor with aluminium foam,” *Int. J. Hydrogen Energy*, vol. 32, no. 14, pp. 2957–2964, Sep. 2007.

[26] B. Satya Sekhar, S. P. Pailwan, and P. Muthukumar, “Studies on metal hydride based single-stage heat transformer,” *Int. J. Hydrogen Energy*, vol. 38, no. 17, pp. 7178–7187, Jun. 2013.

[27] V. Hovland, "*Integrated cabin and fuel cell system thermal management with a metal hydride heat pump"*. National Renewable Energy Laboratory. Citeseer. 2004. Available at: http://www.osti.gov/bridge.

[28] C. Veerraju and M. Ram Gopal, “Heat and mass transfer studies on plate fin-and-elliptical tube type metal hydride reactors,” *Appl. Therm. Eng.*, vol. 30, no. 6–7, pp. 673–682, May 2010.

[29] I. H. Bell, J. Wronski, S. Quoilin, V. Lemort. "*Pure and pseudo-pure fluid thermophysical property evaluation and the opensource thermophysical property library CoolProp*". Ind. Eng. Chem. Res. , vol. 53, no 6, pp. 2498-2508, 2014.

[30] T. Førde, J. P. Maehlen, V. A. Yartys, M. V Lototsky, and H. Uchida, “Influence of intrinsic hydrogenation/dehydrogenation kinetics on the dynamic behaviour of metal hydrides : A semi-empirical model and its verification,” *J. Hydrog. Energy*, vol. 32, pp. 1041–1049, 2007.

[31] American Society of Mechanical Engineers (A.S.M.E.), “Boiler and pressure vessel code section XI”, 1995.